Effects of titanium particle size on osteoblast functions *in vitro* and *in vivo*

Moon G. Choi*, Hae S. Koh*, Daniel Kluess†, Daniel O'Connor†, Anshu Mathur‡, George A. Truskey‡, Janet Rubin§, David X. F. Zhou†, and K.-L. Paul Sung*†¶‖

Departments of *Orthopedic Surgery and †Bioengineering and ¶The Whitaker Institute of Biomedical Engineering, University of California at San Diego, 9500 Gilman Drive, La Jolla, CA 92093; ‡Department of Biomedical Engineering, Duke University, Durham, NC 27708; and §Department of Medicine, Emory University School of Medicine and Veterans Affairs Medical Center, Atlanta, GA 30033

Communicated by Yuan-Cheng B. Fung, University of California at San Diego, La Jolla, CA, February 5, 2005 (received for review May 4, 2004)

The formation of titanium (Ti)-wear particles during the lifetime of an implant is believed to be a major component of loosening due to debris-induced changes in bone cell function. Radiographic evidence indicates a loss of fixation at the implant–bone interface, and we believe that the accumulation of Ti particles may act on the bone-remodeling process and impact both long- and short-term implant-fixation strengths. To determine the effects of various sizes of the Ti particles on osteoblast function *in vivo*, we measured the loss of integration strength around Ti-pin implants inserted into a rat tibia in conjunction with Ti particles from one of four size-groups. Implant integration is mediated primarily by osteoblast adhesion/focal contact pattern, viability, proliferation and differentiation, and osteoclast recruitment at the implant site *in vivo*. This study demonstrates the significant attenuation of osteoblast function concurrent with increased expression of receptor activator of nuclear factor κB ligand (RANKL), a dominant signal for osteoclast recruitment, which is regulated differentially, depending on the size of the Ti particle. Zymography studies have also demonstrated increased activities of matrix metalloproteinases (MMP) 2 and 9 in cells exposed to larger Ti particles. In summary, all particles have adverse effects on osteoblast function, resulting in decreased bone formation and integration, but different mechanisms are elicited by particles of different sizes.

implant stability | focal contact | integration strength | receptor activator of nuclear factor κB ligand | matrix metalloproteinase

Aseptic loosening is emerging as the most common cause of failure for total joint replacements (1, 2). The condition is characterized by an area of osteolysis found at the bone–prosthesis interface and can be identified radiographically as the presence of radiolucent zones at the bone–implant interface (3–6). Previously, aseptic loosening was thought to be a purely mechanical event resulting from the instability of the prosthesis (7–9). However, a biological mechanism of aseptic loosening has recently been proposed that focuses on the bone–prosthesis interface (10, 11). To gain insight into the mechanisms by which particular wear debris induces osteolysis, a number of investigators have studied tissue from revision-surgery patients who have developed aseptic loosening (12–14). Willert and coworkers (15) have reported that the release of wear debris into the bone–implant bed leads to the development of a foreign-body reaction. This reaction is often made worse by repetitive exposure to the foreign substance.

In conjunction with the recent literature (16) describing the evidence of abrasion and burnishing in failed cementless implants, the particles generated from micromotion between bone and implant in the femoral bone bed at the bone–implant interface are believed to be the major cause of numerous osteoblast functional changes that eventually result in improper participation of bone-bed formation and remodeling (16).

Evaluation of the bone–metal interface in terms of bone ongrowth has been limited to a few *in vivo* methods (17–20). Metallic devices of a particular design are implanted in animal models and retrieved at set periods after implantation. One parameter frequently used in our measurements is pull- or push-out strength, which reflects the strength of fixation and, consequently, bone ongrowth (14, 21).

The effects of debris presence in bone and surrounding tissue have been tested directly by osteoclastic cells in contact with particles (22) and indirectly by the quantification of potent osteolytic factors produced by particle-loaded macrophages, lymphocytes (23, 24), and giant cells (25). Although osteoblasts are one of the first cell lines exposed to debris from the prosthesis, the effects of wear-particle size on osteoblasts have not been closely investigated. Cytokines (from monocytes and macrophages) and matrix metalloproteinases (MMPs) (from fibroblasts) can affect the attachment (26, 27) and synthetic (28, 29) activities of osteoblasts and cause the reduction of bone matrix and mineral deposition (24, 30). Ti particles can also induce local bone remodeling by osteoclast recruitment through increased expression of receptor activator of nuclear factor κB ligand (RANKL) on osteoblasts. These functional changes of osteoblasts can influence bone-bed remodeling and ongrowth around the implant site. Thus, to characterize the contribution of catabolic processes to remodeling, *in vitro* zymographic tests were performed to evaluate the matrix activity of MMP-2 and MMP-9, two proteolytic activities involved in the degradation of the organic matrix in bone bed.

The overall objective of this study was to assess the effect of various sizes of Ti particles on bone ongrowth and implant fixation *in vivo* and *in vitro*. After loading various sizes of Ti particles into the implant-insertion site, the integration strength in the animal model was measured, and the degree to which particles obstructed bone ongrowth and osteoblast function was evaluated. Variations in MMP activity, RANKL expression, and osteoblast viability and proliferation among control and experimental groups were used as mechanisms by which to measure how differently sized Ti particles affected implant integration. Potential bone defects and the quality of the bone–implant interface were also assessed during the microscopic visualization of the insertion site after pin extraction.

Materials and Methods

Size Profiling, Composition, and Concentration of Ti Particles. Pure Ti particles were purchased from Alfa Aesar (Ward Hill, MA) in a 25 g/100 ml of water mixture, with 90% of the particles <20 μm in size. The particles were suspended in deionized distilled (DD) H_2O, vortexed, and separated according to the variable sedimentation rates of the variously sized particles. After sedimentation, the size distribution of the particles was examined under video-enhanced oil-immersion-lens microscopy (×4,000). The sedimentation procedure was repeated until $>90\%$ of the particles were within the

Abbreviations: FDA, fluorescein diacetate; MMP, matrix metalloproteinase; PI, propidium iodide; RANKL, receptor activator of nuclear factor κB ligand; TIRFM, total internal reflection fluorescence microscope.

‖To whom correspondence should be addressed at: Orthopedics and Bioengineering, 0412, University of California at San Diego, 9500 Gilman Drive, La Jolla, CA 92093-0412. E-mail: klsung@ucsd.edu.

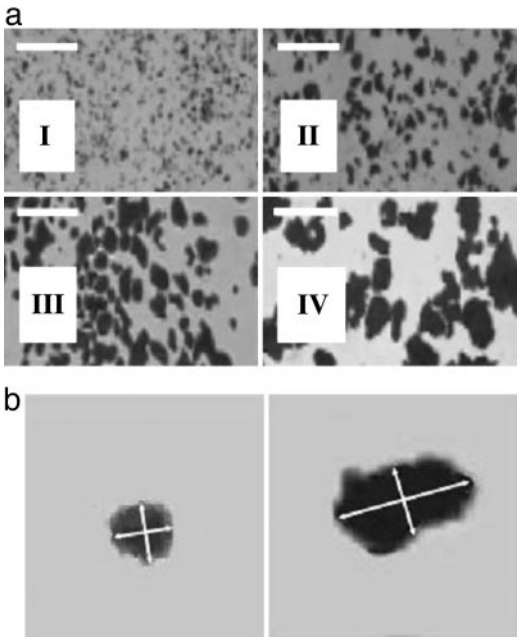

Fig. 1. Particle size separation. (*a*) Alfa Aesar Ti particles: <1.5 μm (group I), ≥1.5 μm and <5.0 μm (group II), ≥5.0 μm and <10.0 μm (group III), and ≥10.0 μm and <15.0 μm, (group IV). (Scale bars, 20 μm.) (*b*) *Left* is an enlargement of a particle from *aI*, illustrating axial measurements (indicated by arrows) used in size determination of particles from group I. *Right* is an enlargement of a particle from *aIV*, illustrating axial measurements of a particle from group IV. The ratio of long to short axial measurement is 1 (*Left*) and 2 (*Right*).

desired size-group. The desired size-group was determined by taking the mean of the particle's maximum length and minimum width. The size-groups (I, II, III, and IV) were selected according to the size of the osteoblast cell. Three smaller particle sizes were chosen for phagocytosis (<1.5 μm, ≥1.5 μm and <5.0 μm, and ≥5.0 μm and <10.0 μm) and one larger size (≥10 μm and <15.0 μm) to serve as a control (Fig. 1). After separation, the particles were boiled in 1% acetic acid for 90 min, washed three times with DD H_2O, and autoclaved at 135°C for 3 h to minimize endotoxin contamination. In preparation for pin integration, the particles were air-dried and resuspended in PBS to a concentration of 5 wt % Ti. The Ti suspensions were then sonicated for 30 min immediately before the insertion.

Pin Material and Location. Smooth Ti alloy (Ti-6Al-4V) cylindrical wire with a 1.2-mm outer diameter was cut into rods 3.5 mm long. The rod ends were sanded with 330-mesh sandpaper, and a notch was made at one end for attachment to the step-force loading apparatus during pin extraction. Each pin was carefully examined under the dissecting microscope to ensure a smooth surface and equal implant length. Implant pins were rinsed in 70% ethanol and autoclaved before insertion. To determine the optimal pin-insertion point, we screened four implant locations on the tibia. A Dremel bit (outer diameter 1.5 mm) was used to drill a series of holes along the tibia on the medial side from the proximal to the distal point of the bone. Three holes were made, at ≈12, 8.5, and 4.8 mm from the most prominent point of the tibial crest on the proximal side. Another hole was made 1 mm below and distal to the prominent point of the tibial crest. The three proximal holes were 3.0–3.4 mm deep, and the single distal hole was 1.5–2.5 mm deep. The magnitude of pull-out force varies with the locations of the pins. A medial insertion parallel to the articulating surface of the knee and 7 mm above the most prominent part of the tibial crest was found to provide the most consistent degree of integration, the most optimal for this study. This protocol involved the use of adult Wistar rats and was approved by the Animal Subjects Committee at the University of California at San Diego.

Implantation Procedure. Forty-four adult Wistar rats (≈400 g) were anesthetized with sterile pentobarbital (50 mg/kg). The medial side of each tibia (from the knee-joint line to the prominent portion of the tibial crest) was exposed. Four holes were drilled into each tibia under a dissecting microscope at the predetermined locations (see previous section). Four suspensions of Ti particles in PBS were prepared. On the experimental leg, 3 μl of a PBS suspension containing 5 wt % Ti particles in one of four different size ranges (<1.5 μm, ≥1.5 μm and <5.0 μm, ≥5.0 μm and <10.0 μm, and ≥10.0 μm and <15.0 μm) were injected into the spaces surrounding the four pins. An equivalent volume of PBS was injected into the opposite leg as the control. The Ti pins were subsequently inserted into the holes, and the subjects were allowed to recover. On days 30 and 41 after the procedure, 44 and 18 rats, respectively, with pins in different locations but without particles, were killed.

Determination of Integration Force and Integration Strength. The tibia was dissected and anchored in a clamp to maintain a vertical orientation normal to the medial surface. At a step-loading rate of 1 N/15 s to determine the pull-out force, the tibia was kept in place, and weights were added until the pin was dislocated from the bone. After dislocation, the tibias were cross-sectioned at the integration site. The site was carefully measured under a dissecting microscope and photographed with a charge-coupled device camera to record the degree of bone ongrowth by using National Institutes of Health software program IMAGE. The integration area was calculated with the measured pin diameter and insertion depth, and the degree of ongrowth was subtracted from the total surface area. Integration force and integration strength were calculated by normalizing the integration area with respect to the control group.

Total Internal Reflection Fluorescence Microscope (TIRFM) Studies of Osteoblasts. A 4.1- × 4.7-cm anodized aluminum plate milled with a 3.8- × 1.8-cm opening and 0.1-cm thickness was sealed to the cell-plated coverslip surface by a layer of silicon lubricant (Dow Corning, Midland, MI) and then secured with screws to the 12.3- × 7.2-cm fluid cell. This produced a 0.2-cm-deep liquid reservoir into which growth medium was added to maintain cell viability. The medium was changed periodically to control the temperature and pH. The ends of the slides were cleaned with lens paper immersed in 70% ethanol to remove growth medium and cell debris from the surface. A small drop of coupling oil (refractive index $n = 1.515$; Cargill Labs, Cedar Grove, NJ) was placed on one end of the coverslip to accommodate the coupling prism (BK-7 glass, $n = 1.515$; Karl Lambertech, Chicago). The entire assembly was fixed to the stage of the TIRFM apparatus, which was secured to the stage of an inverted microscope (Zeiss Axiovert 100 TV inverted microscope).

DiI Carbocyanine Dye Staining. Before being plated, cells were labeled with DiI, a carbocyanine dye that partitions into the cell membrane. The cells were cultured overnight on fibronectin-coated surfaces. Cells from groups I and II were incubated with Ti (0.05%) for 4 h, whereas the control group was not.

Osteoblast-Proliferation Assay (Promega CellTiter Assay). Initial cell populations were calculated after trypsinization, and 20,000 cells per well were seeded onto a 96-well UV spectrophotometer plate. Total volume of medium, cells, and Ti particles was 200 μl per well. At least three wells and two replicates were prepared for each combination of variables. A number of cell/Ti-particle-loading techniques were tested (data not shown). Simultaneous loading provided the most consistent results and was, therefore, selected for this experiment.

Relative proliferation data (0.1 wt % particle compared with 0 wt

% control) were collected at 72 h after loading with Promega CellTiter one-step assay. CellTiter was added to the cell culture for a final concentration of 1:5 reagent to medium. The cells were incubated, and the dye was allowed to develop for 90 min. The medium/reagent mixture was removed to a 96-well spectrophotometer reader plate and centrifuged for 7 min at 200 × *g* to pellet cellular debris and any contaminated Ti particles. The supernatant was collected in clean wells on the 96-well plate and read at 650 nm (background) and 490 nm (CellTiter reagent absorbance) by using an EMax spectrophotometer (Molecular Devices). The dye demonstrated a linear relationship between absorbance at 490 nm and viable cell population.

Osteoblast-Viability Assay with Fluorescein Diacetate (FDA)–Propidium Iodide (PI) Staining. Viability data were collected after trypsinizing the particle-loaded cells for 72 h and preparing them for visualization with FDA and PI. Cells were prepared after cell culture medium was removed, and the cells were washed twice with warmed PBS. The medium and washes were collected in a microcentrifuge tube to ensure that no dead cells were discarded before staining. Cells were then trypsinized with 300 μl of trypsin solution and incubated for 3 min. The trypsin–cell mixture was then added to the microcentrifuge tube containing the medium and PBS and centrifuged at 200 × *g* for 5 min. The supernatant was carefully removed, and the pellet was resuspended in 200 μl of FDA and 200 μl of PI working solutions (25 μg of FDA per ml of PBS and 1 mg of PI per ml of PBS). Cells were incubated in the solution for 4–5 min and then visualized by UV microscopy at 510 nm (green, live) or 546 nm (red, dead) for cell counts. Approximately 150 cells were counted per field with a total of 12 fields viewed for each data point.

Real-Time PCR for RANKL mRNA and 18S rRNA Expression. ST2 cells were plated at 10^5 per well in six-well plates with vitamin D-excluded culture medium. Control groups consisted of cells in culture medium alone, whereas experimental groups consisted of cells in medium containing 0.1 wt % Ti particles in one of the following three size-groups: <1.5, ≥1.5 and <5.0, and ≥5.0 and <10.0 μm (groups I, II, and III, respectively). ST2 cells were exposed to Ti particles for a total of 24 and 48 h. Total RNA (0.5 μg) from ST2 cells was reverse-transcribed with primers for RANKL and 18S RNA, followed by PCR in the presence of SYBR green, and the cycle threshold was assessed. Standards and samples were run in triplicate. RANKL was normalized for the amount of 18S in the reverse-transcribed sample, which was also standardized on a dilution curve from a control reverse-transcribed sample (31). The primers specific for RANKL and 18S and the methods of analysis used were similar to those described in refs. 32 and 33. Amplicon 150-bp forward and reverse of RANKL primers were 5′-CAC CAT CAG CTG AAG ATA GT and 5′-CCA AGA TCT CTA ACA TGA CG, respectively. Real-time analysis was performed on a Bio-Rad iCycler with SYBR green as readout. Control cell RANKL and 18S reached thresholds between cycles 22–26 (94°C, 56°C, and 72°C cycles per 30 sec). From the relative standard curves for control RNA and 18S RNA, the efficiencies of reactions for both RANKL and 18S RNA were found to be >90%.

Zymography Assay. Studies of MMP-2 and MMP-9 activities in rat osteoblasts exposed to Ti particles were done *in vitro* by using the same size-groups of particles. One-half-million osteoblasts from passages 3–5 were cultured in a 24-well plate in 10% FBS high-glucose complete DMEM containing different concentrations (0.01 wt %, 0.05 and 0.1 wt %) of each size-group of particles. Two additional wells without particles were seeded as controls. The activities of MMP-2 and MMP-9 were examined at time steps of 8, 24, 48, and 72 h by gelatin zymography (34). The samples were run on a polyacrylamide gel made with the addition of gelatin, which is a substrate of MMP-2 and MMP-9. Once the samples were loaded, the enzymes were allowed to digest the gelatin. The gel was subsequently stained with Coomassie blue (0.25%) to detect the presence of MMP-2 and MMP-9, which was reflected in the unstained regions of the gel where the protein (gelatin) level was low because of the digestion of gelatin by MMP-2 and MMP-9.

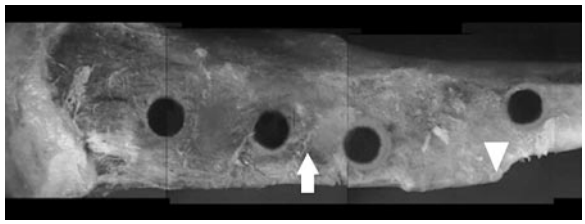

Fig. 2. Rat tibias with multiple insertion sites. The arrow indicates the selected position for pin insertions (7 mm proximal to the prominent point on the tibial crest). This location provided the optimal and most consistent integration when measured by extraction force. The arrowhead indicates the prominent portion of the tibial crest from which measurements were made. The holes, from left to right, are 12, 8.5, 4.8, and −1 mm relative to the point on the tibial crest (left leg).

Results

Particle Separation. The size of each particle was determined by taking the mean of its long axial length and short axial width (see Fig. 1*b*). Subsequently, we sorted all particles into four groups according to size: group I, <1.5 μm; group II, ≥1.5 μm and <5.0 μm; group III, ≥5.0 μm and <10.0 μm; and group IV, ≥10.0 μm and <15.0 μm. Separation results were verified by video-enhanced oil-immersion lens microscopy (×4,000), which confirmed that >98% of particles in group I and >80% of particles in group IV were within the desired size range (Fig. 1).

Location of Pin Insertion. In a preliminary study, we examined the effects of pin depth, cortical thickness, the density of spongy (trabecular) bone, and duration of incubation on integration strength. The results from this study showed a uniform pin depth in the proximal three holes and less depth in the distal fourth hole (Fig. 2). The integration force of mixed-size-particle experiments measured by step loading was higher in the middle two holes than in the other holes (Table 1). The pin inserted with mixed-size particles at the middle of the bone for 41 d (7.8 mm above the prominent point of the tibial crest) had uniform insertion length and integration strength with less variance than the other pin placements (Table 1) and, therefore, was used as the insertion point for subsequent implant procedures.

Gross Description of Pin Insertion Site. The pins were surrounded by thin callus-like new bone in all cases. No difference in the callus bone among experimental groups and the control was found. The control groups had a smooth surface and complete bone ongrowth with no sign of defects or incomplete growth shown in the cross

Table 1. Preliminary study of integration force and strength of tibial implants (without Ti-particle loading) at different locations after 41 d (mean ± SD)

Proximal distance from tibial crest,* mm	Insertion length, mm	Integration force, N	Integration strength, N/mm²
11.5 (n = 5)	2.7 ± 0.2	8.56 ± 5.05	1.04 ± 0.61
7.8 (n = 5)	2.7 ± 0.1	9.40 ± 3.22	1.13 ± 0.33
4.8 (n = 4)	3.8 ± 0.4	12.5 ± 3.50	0.88 ± 0.31
−1 (n = 4)	1.6 ± 0.2	1.25 ± 0.35	0.36 ± 0.22

*Distance above and below tibial crest is reflected by positive and negative values, respectively.

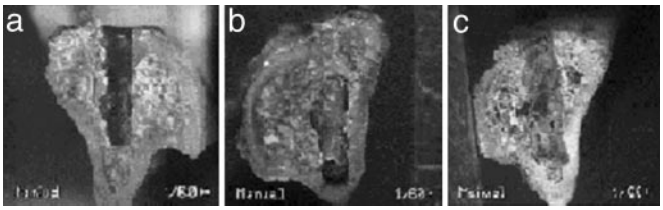

Fig. 3. Cross section of the proximal portion of a rat tibia. Distances proximal to the prominent point on the tibial crest and medial to the tibial crest are 8.1 ± 0.62 mm and 2.2 ± 0.27 mm, respectively (mean ± SD). Insertion depth and pull-out force for each particle-size-group are from control (no particles; 3.8 mm, and 9.44 N) (*a*), ≥1.5 μm and <5.0 μm (4 mm and 8.4 N) (*b*), and ≥5.0 μm and <10.0 μm (4 mm and 10.62 N) (*c*), respectively. Pin extraction was performed at 41 d after implantation.

section. Experimental legs exhibited various bone defects around the newly formed areas of bone ongrowth (Fig. 3).

Integration Force and Integration Strength Determination. In all groups presented in Table 2, smaller forces were required to extract pins from experimental legs (loaded with particles) than from control legs. The <1.5 μm, ≥1.5 μm and <5.0 μm, ≥5.0 μm and <10.0 μm, and ≥10.0 μm and <15.0 μm size-groups had 36%, 60%, 36%, and 34% of the integration strength of the control group, respectively.

TIRFM Studies of Osteoblast Adhesiveness. Like other attached cells, focal contacts of osteoblasts were located near the cell periphery. Focal contacts were extremely stable after application. Osteoblasts treated with Ti particles appeared to be in disorganized random arrangement and had fewer focal contacts than did control cells (Fig. 4).

Osteoblast Proliferation Assay. The data shown (Fig. 5) represent results from three wells prepared for each particle size ($n = 5$). Our figures depict data from the 0.1 wt % proliferation studies at 72 h under conditions of loading with all four particle-size-groups and control, normalized relative to the control group of untreated cells from each time interval. A significant decrease in proliferation for all groups was shown.

Osteoblast Viability Assay. The results from the 72-h viability assays by FDA–PI staining and fluorescent microscopy examination are depicted in Fig. 5. At least 150 cells were counted in each of six fields per data point (two replicates) and analyzed for these results. Ti particles were clearly visible in the cytoplasm of the <1.5 μm and the ≥1.5 μm and <5.0 μm size-groups (I and II). The ≥10.0 μm and <15.0 μm size-group (IV) had no visible phagocytosed cells; rather, these particles appeared too large to be internalized and were, instead, attached to the plasma membrane of the viable cells. Some particles of the ≥5.0 μm and <10.0 μm size-group (III) were

Table 2. Integration strength at 7.8 ± 0.5 mm above tibial crest location under conditions of Ti-particle loading for 30 d (mean ± SD)

Particle size group, μm	Insertion length, mm	Integration force, N	Integration strength, N/mm²
Control ($n = 26$)	2.95 ± 0.44	9.04 ± 3.40	0.90 ± 0.25
<1.5 ($n = 7$)	3.10 ± 0.24	4.21 ± 1.58	0.40 ± 0.16*
≥1.5 and <5.0 ($n = 7$)	2.90 ± 0.38	6.63 ± 1.37	0.67 ± 0.14*
≥5.0 and <10.0 ($n = 5$)	2.92 ± 0.22	4.00 ± 0.91	0.40 ± 0.07*
≥10.0 and <15.0 ($n = 7$)	2.71 ± 0.27	3.57 ± 1.40	0.38 ± 0.15*

*Significant relative to the control group; $P < 0.05$.

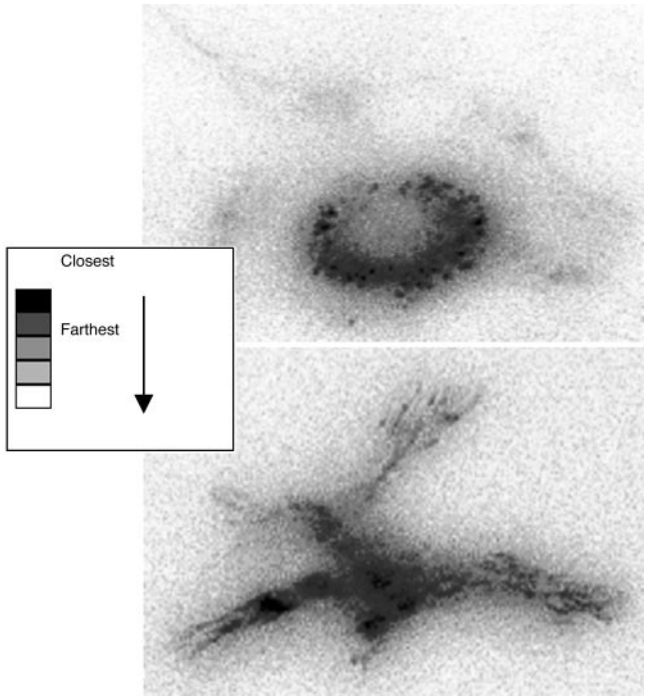

Fig. 4. Focal contact arrangement of normal osteoblast (*Upper*) in a well organized peripheral arrangement vs. Ti-treated osteoblast (*Lower*) in an unorganized random arrangement.

present within the cytoplasm, whereas other particles in the same group attached themselves to the outside surface of plasma membrane. Consistent with these observations, a significant decrease in viability was confirmed for all groups, with the exception of group IV.

Real-Time PCR Analysis of ST2 Cells for RANKL Expression. The levels of RANKL expression in cells loaded with a 0.1 wt % Ti-particle-loaded cell-culture medium were compared with a control, non-particle-loaded cell-culture medium in each of three size-groups; <1.5 μm, ≥1.5 μm and <5.0 μm, and ≥5.0 μm and <10.0 μm. Data from this study are represented in Fig. 6. Particles in the ≥5.0

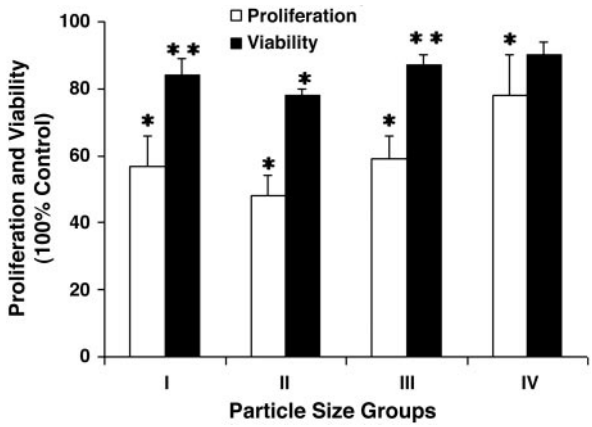

Fig. 5. Effects of Ti-particle size on osteoblast proliferation and viability at 0.1 wt % for 72 h ($n = 5$). Four groups are particle size <1.5 μm (group I), ≥1.5 μm and <5.0 μm (group II), ≥5.0 μm and <10.0 μm (group III), and ≥10.0 μm and <15.0 μm (group IV), measured as percentage of proliferation and viable cells, normalized relative to control (without particle loading). Error bars, ±SD. *, Proliferation study done with $P < 0.01$; **, viability study done with $P < 0.05$.

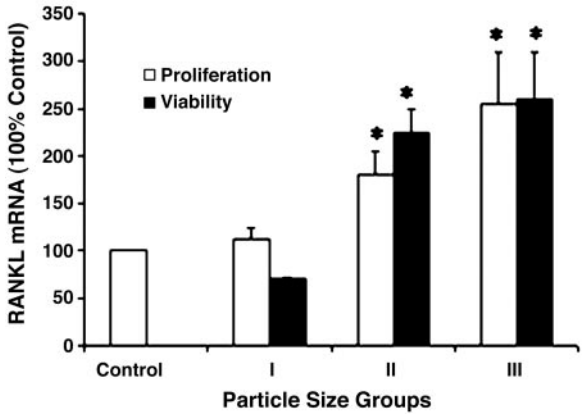

Fig. 6. Plot of real-time PCR data of RANKL levels after loading with 0.1 wt % Ti particles of three size-separated groups (relative to control) for 24 and 48 h. The number of assays measured for each data point ranges from $n = 10$ to $n = 4$. Error bars, ±SEM. *, $P < 0.01$ compared with control.

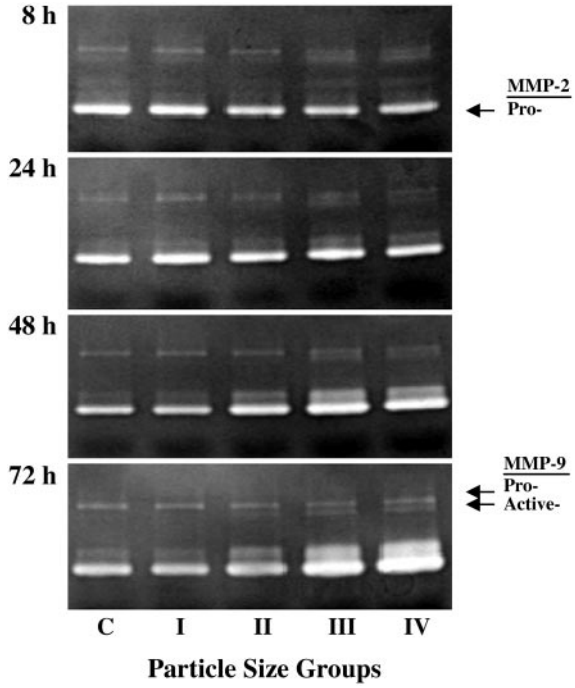

Fig. 7. Results from zymography. The results present a clear increase in MMP-2 activity in groups III and IV at 48 and 72 h, but small particles (groups I and II) have no effect at 8 and 24 h. MMP-9 pro- and active-form activities are increased at 48- and 72-h incubation periods. (Particle concentration 0.01 wt %.)

μm and <10.0 μm size-group caused the highest expression (2.5 times that of control cells), and particles in the <1.5 μm size-group had no significant effect on RANKL expression. Ti particles in the midsize-group (≥1.5 μm and <5.0 μm) doubled the RANKL-expression level, compared with the control. The levels attained by the largest-size particles are equivalent to RANKL mRNA induced by 1 nM vitamin D (data not shown). The effect on RANKL expression was maximal after the first 24 h and did not continue to increase with 24 h of additional exposure. This result may suggest that the particle effect was not due to the secretion of a secondary mediator of RANKL expression.

Zymography Analysis. The results of the MMP-2 and MMP-9 study show clear relationships among particle size (0.01 wt %), incubation time, and proteolytic activity (Fig. 7). There was a noticeable difference among the control group and groups III and IV (Fig. 7). The activities of MMP-2 and pro- and active-forms of MMP-9 also increased at 48 and 72 h in groups III and IV (Fig. 7). The active form (groups III and IV) of MMP-9 at 72 h was significantly increased over the control group, but no difference was observed among the control group and groups I and II. Other concentrations of Ti particles (0.05% and 0.1%) also had a significant effect on proteolytic activity (data not shown), consistent with patterns obtained with 0.01 wt %.

Discussion

This study clearly demonstrates that the integration strength due to bone ongrowth around a Ti-pin implant is adversely affected by the presence of Ti particles and that the adverse effect varies with the particle size. The pits and defects seen at the bone-integration site in the experimental groups are believed to be the result of direct and indirect effects of Ti-particle loading on osteoblasts and osteoclasts, respectively. Despite the excellent biocompatibility characteristics of Ti in bulk form (35), the adverse effects of Ti particles on osteoblast function have been characterized by a number of researchers (11, 36, 37). The gross reduction in implant-integration strength may be the result of a number of tissue responses in the periprosthetic bone bed, mediated, at least in part, by osteoblasts, whose proper function is critical to successful bone-tissue ongrowth and, therefore, integration strength. Results from TIRFM studies suggest that the difference in contact area between control and Ti-particle-treated osteoblasts may explain the reduced adhesion after ingestion of Ti particles. Ti-treated osteoblasts showed a disrupted focal adhesion arrangement and no clear nuclear region, as compared with the untreated osteoblasts. The focal adhesion and stress fiber arrangement were clearly disrupted, compared with untreated cells, and may have contributed to the reduced adhesion force in Ti-treated osteoblasts (28). Furthermore, results from our studies support the hypothesis that all sizes of particles (not limited to groups I and II) are obstacles to normal osteoblast function. In our *in vitro* proliferation and viability experiments, the Ti particles having the most harmful effect on osteoblast function were groups I, II, and III (38). The lowered integration strength in these groups could be the result of specific events triggered by phagocytosis, and that caused by the largest particle size ≥10 μm and <15.0 μm (group IV) through a separate mechanism of stereohindrance. The large size and high concentration of large particles prevent the integration of the pin by physically retarding the formation of a secure implant–bone interface at the extracellular level rather than by phagocytotic activities. In addition, this group of particles can be phagocytosed by osteoclasts, cells that can increase bone absorption.

The most common sizes of metal particles found in the retrieval studies after total joint replacement were 1–10 μm (39), and this metallic-wear debris can disseminate to systemic organs of the body (40). Recently, it has been shown that proinflammatory cytokines (i.e., TNF-α and interleukins-1 and -6) are released after phagocytosis by resident macrophages and the development of an erosive pannus that stimulates bone resorption by osteoclasts (41). It is also known that bone resorption and the differentiation of macrophages into bone resorbing osteoclastic cells are more extensive in the presence of metal-particulate debris (40, 42). Therefore, the presence of Ti particles can elicit osteolytic responses from both osteoclasts and osteoblasts in bone tissue.

The murine stromal cell line ST2 is an indicator of cellular responses from primary osteoblasts and is well known to respond to osteoactive factors such as vitamin D (43) and TNF-α (44) with regulated RANKL mRNA expression (45). Because debris wear can induce local bone remodeling by recruiting osteoclasts through the regulation of RANKL expression (43), RANKL mRNA ex-

pression of ST2 cells in response to particle loading was explored by a quantitative real-time PCR assay in the present study.

We found that the ST2 cells in their basal state express very low levels of RANKL and do not support osteoclastogenesis until treated with osteoclastogenic factors such as vitamin D (43). Ti-particle loading increased RANKL expression to significant levels. Particles of >1.5 μm caused significant increases in RANKL expression with increased response to the largest Ti-particle group. These results suggest that ST2 cells recognize particle size, and particles of >1.5 μm cause a response consistent with the initiation of local bone remodeling. Although the smaller particle size did not cause noticeable changes in RANKL expression, osteoblast cell function was impacted in other ways. In our *in vitro* study, proliferation results showed that particles of <1.5 μm cause significant inhibition ($>40\%$ by 0.1% particle loading) and viability decrease (15% for 72-h loading). Also, in our *in vivo* study, particles of this size-group inhibited bone ongrowth and recovery by 40% after loading particles with pin insertion. Hence, Ti particles of different sizes appear to be able to generate different functional responses in bone osteoblast and stromal cells.

Our previous osteoblast biorheological studies indicate that phagocytosed Ti particles and actin filaments form a complex in the cytoskeleton, which, in turn, decreases cellular adhesion and cell spreading and, therefore, cellular-attachment area (28). Attachment-dependent cells, including osteoblasts, rely on interactions with extracellular substrates to maintain critical cell functions such as proliferation, expression of structural and adhesive proteins (type I collagen and fibronectin, respectively), and other activities related to cell viability and apoptotic behavior. It is reasonable to attribute a large degree of the loss of implant-integration capability of particle-loaded bone tissue *in vivo* to these effects of the particle loading of osteoblasts *in vitro*. A decrease in osteoblast viability, adhesion, protein secretion, and proliferation would greatly reduce the capability of the cell to integrate with an otherwise biocompatible implant, and it is the attenuation of these functions to which we attribute the reported loss of integration force.

The study of the activity of MMP-2 and MMP-9 demonstrated that an increase in the proteolytic activity of MMP-2 protein occurred with increasing particle size at 48 and 72 h. Increased size of particles (group III) or large particles (group IV) can change cellular adhesive behavior, which can significantly activate MMP activities. Cells exposed to particles in the size range ≥ 1.5 μm and <5.0 μm had less activity than control cells, but the activity at larger particle sizes from 5.0 μm to 15.0 μm is increased relative to the control. The MMP-9-active-form study shows an obvious dependency on particle sizes in 48- and 72-h collections. This deterioration of bone-matrix proteins would be an obstacle to bone formation at the site of bone ongrowth and cause a decrease in integration strength.

The most frequently observed feature of the periprosthetic bone tissue in failed total joint arthroplasties is a bone surface with evidence of substantial defects and resorption (30). Examination of cementless implants retrieved from failed arthroplasties indicates that significant scoring and burnishing of the implant surface can release a large number of Ti particles in a short period after implantation (16). It is reasonable to conclude that Ti-wear particles generated at this interface are likely to contact the bone-forming cells around loose implants. If functions of osteoblasts, such as viability, proliferation, differentiation, and production of bone formation-related proteins are suppressed by wear particles, the bone growth–bone resorption equilibrium mediated by osteoblasts and osteoclasts will be disturbed, resulting in a net reduction of bone mass and ongrowth. This study highlights the association between pin implants and the size of particles, which increase the potential for osteolysis. Increased awareness of this destructive process is becoming more important with the growing aging-related popularity of total hip and knee arthroplasty.

We thank Ms. Tamara Murphy, Mr. Erick Lu, Mr. Jay Kim, Ms. Chuan Qin, and Ms. I-wen Wang for technical support. This work was supported by the Bristol-Myers/Zimmer Award for Excellence in Orthopaedic Research and National Institutes of Health Grant AR 14918.

1. Clarke, I. C., Campbell, P. & Kossovsky, N. (1992) *Amer. Soc. Test. Mat. Spec. Tech. Pub.* **1144,** 7–26.
2. Friedman, R. J., Black, J., Galante, J. O., Jacobs, J. J. & Skinner, H. B. (1993) *J. Bone Jt. Surg. Am. Vol.* **75A,** 1086–1109.
3. Engh, C. A., Massin, P. & Suthers, K. E. (1990) *Clin. Orthop. Rel. Res.* **257,** 107–128.
4. Kobayashi, A., Donnelly, W. J., Scott, G. & Freeman, M. A. (1997) *J. Bone Jt. Surg. Br. Vol.* **79,** 583–589.
5. Santavirta, S., Hoikka, V., Eskola, A., Knottinen, Y. T., Paavilainen, T. & Tallroth, K. (1990) *J. Bone Jt. Surg. Br. Vol.* **72,** 980–984.
6. Wang, J. T., Harada, Y., Goldring, S. R. (1992) *Sem. Arthroplasty* **4,** 215–222.
7. Goldring, S. R., Jasty, M., Roelke, M. S., Rourke, C. M., Bringhurst, F. R. & Harris, W. H. (1986) *Arthritis Rheum.* **29,** 836–842.
8. Linder, L., Lindberg, L. & Carlsson, A. (1983) *Clin. Orthop.* **175,** 93–104.
9. Partson, M., Fulford, P. & Denham, R. (1986) *J. Bone Jt. Surg. Br. Vol.* **68,** 392–397.
10. Appel, A. M., Sowder, W. G., Siverhus, S. W., Hopson, C. N. & Herman, J. H. (1990) *Br. J. Rheumatol.* **29,** 32–36.
11. Jasty, M. & Smith, E. (1992) *Curr. Opin. Rheumatol.* **4,** 204–209.
12. Bennett, N. E. & Goldring, S. R. (1990) *Arthritis Rheum.* **33,** S115.
13. Cook, S. D., McCluskey, L. C., Martin, P. C. & Haddad, R. J. (1991) *Clin. Orthop.* **264,** 209–222.
14. Cook, S. D., Thomas, K. A. & Haddad, R. J. (1988) *Clin. Orthop.* **234,** 90–101.
15. Willert, H. G., Bertram, H. & Buchhorn, B. H. (1990) *Clin. Orthop. Rel. Res.* **258,** 95–107.
16. Maccauro, G., Piconi, C., Pilloni, L., Proietti, L., De Santis, V. & De Santis, E. (2000) *Int. Orthop.* **24,** 231–233.
17. Bobyn, J. D. & Engh, C. A. (1984) *Orthopaedics* **7,** 1410–1422.
18. Bobyn, J. D., Pilliar, R. M., Cameron, H. U. & Weatherly, G. C. (1981) *Acta Orthop. Scand.* **52,** 145–153.
19. Cook, S. D., Scheller, A. D., Anderson, R. C. & Haddad, R. J. (1985) *Clin. Orthop.* **202,** 147–151.
20. Haddad, R. J., Cook, S. D. & Thomas, K. A. (1987) *J. Bone Jt. Surg. Am. Vol.* **69,** 1459–1466.
21. Dohmae, Y., Bechtold, J. E., Sherman, R. E., Puno, R. M. & Gustilo, R. B. (1988) *Clin. Orthop.* **236,** 303–312.
22. Urban, R. M., Jacobs, J. J., Tomlinson, M. J., Gavrilovic, J., Black, J. & Peoc'h, M. (2000) *J. Bone Jt. Surg. Am. Vol.* **82,** 457–476.
23. Horowitz, S. M., Gautsh, T. L., Frondoza, C. G. & Riley, L., Jr. (1993) *J. Orthop. Res.* **9,** 406–413.
24. Horowitz, S. M. & Gonzales, J. B. (1996) *Calcif. Tissue Int.* **59,** 392–396.
25. Goodman, S. B., Davidson, J. A., Song, Y., Martial, N. & Fornasier, V. L. (1996) *Biomaterials* **17,** 1943–1947.
26. Evans, C. E. & Jones, S. (1988) *Calcif. Tissue Int.* **63,** 496–504.
27. Kwon, S. Y., Takei, H., Pioletti, D. P., Lin, T., Ma, Q. J., Akeson, W. H., Wood, D. J. & Sung, K.-L. P. (2000) *J. Orthop. Res.* **18,** 203–211.
28. Kwon, S. Y., Lin, T., Takei, H., Ma, Q., Wood, D. J., O'Connor, D. & Sung, K.-L. P. (2001) *Biorheology* **38**, 161–183.
29. Yao, J. L., Cs-Szabo, G., Jacobs, J. J., Kuettner, K. & Glant, T. T. (1997) *J. Bone Jt. Surg. Am. Vol.* **79,** 107–112.
30. Kusano, K., Miyaura, C., Inada, M., Tamura, T., Ito, A., Nagase, H., Kamoi, K. & Suda, T. (1998) *Endocrinology* **139,** 1338–1345.
31. Johnson, M. R., Wang, K., Smith, J. B., Heslin, M. J. & Diasio, R. B. (2000) *Anal. Biochem.* **278,** 175–184.
32. Rubin, J., Ackert-Bicknell, C., Zhu, L., Fan, X., Murphy, T., Nanes, M., Marcus, R., Holloway, L., Beamer, W. & Rosen, C. (2002) *J. Clin. Endocrinol. Metab.* **87,** 4273–4279.
33. Rubin, J., Murphy, T., Fan, X., Goldschmidt, M. & Taylor, W. (2002) *J. Bone Miner. Res.* **17,** 1452–1460.
34. Senior, R. M., Griffin, G. L., Fliszar, C. J., Shapiro, S. D., Goldberg, G. I. & Welgus, H. G. (1991) *J. Biol. Chem.* **266,** 7870–7875.
35. Nugiel, D. J., Wood, D. & Sung, K.-L. P. (1996) *Tissue Eng.* **2,** 27–140.
36. Lombardi, A. V., Mallory, T. H., Vaughan, B. K. & Drouillard, P. (1989) *J. Bone Jt. Surg. Am. Vol.* **71,** 1337–1342.
37. Pioletti, D. P., Takei, H., Kwon, S. Y., Wood, D. J. & Sung, K.-L. P. (1999) *J. Biomed. Mater. Res.* **46,** 399–407.
38. O'Connor, D. T., Choi, M. G., Kwon, S. Y. & Sung, K-L. P. (2004) *J. Orthop. Res.* **22,** 229–236.
39. Dorr, L. D., Hilton, K. R., Wan, Z, Markovich, G. D. & Bloebaum, R. (1996) *Clin. Orthop.* **333,** 108–117.
40. Sabokbar, A., Pandey, R., Quinn, J. M. & Athanasou, N. A. (1998) *Arch. Orthop. Trauma Surg.* **117,** 136–140.
41. Schwartz, Z., Lohmann, C. H., Wieland, M., Cochran, D. L., Dean, D. D., Textor, M., Bonewald, L. F. & Boyan, B. D. (2000) *J. Periodontol.* **71,** 586–597.
42. Kadoya, Y., Salmivirta, K., Talts, J. F., Kadoya, K., Mayer, U., Timpl, R. & Ekblom, P. (1997) *Development (Cambridge, U.K.)* **124,** 683–691.
43. Yasuda, H., Shima, N., Nakagawa, N., Yamaguchi, K., Kinosaki, M., Mochizuki, S., Tomoyasu, A., Yano, K., Goto, M., Murakami, A., *et al.* (1998) *Proc. Natl. Acad. Sci. USA* **95,** 3597–3602.
44. Nakashima, T., Kobayashi, Y., Yamasaki, S., Kawakami, A., Eguchi, K., Sasaki, H. & Sakai, H. (2000) *Biochem. Biophys. Res. Commun.* **275,** 768–775.
45. Lee, S. K. & Lorenzo, J. A. (1999) *Endocrinology* **140,** 3552–3561.